Mechanics & Industry **24**, 22 (2023)
© A. Li et al., Published by EDP Sciences 2023
https://doi.org/10.1051/meca/2023022

Mechanics & Industry

Available online at:
www.mechanics-industry.org

REGULAR ARTICLE OPEN ACCESS

# Effects of cutting head load on fatigue life of bolter miner cutting arm

Ang Li[1,*], Bukang Wang[1,2,3], Teng Wang[1,2,3], Zhifu Guo[1,2,3], and Zhaokun Yan[4]

[1] China Coal Research Institute, Beijing, China
[2] CCTEG Taiyuan Research Institute Co., Ltd, Taiyuan, China
[3] China National Engineering Laboratory for Coal Mining Machinery, Taiyuan, China
[4] Taiyuan University of Technology, Taiyuan, China

Received: 1 May 2023 / Accepted: 28 June 2023

**Abstract.** In the operation of bolter miners, the cutting arm is an essential and weak part and its fatigue life directly affects its performance. This study aimed to investigate the influence of the cutting head load on the fatigue life of a cutting arm using the DEM-MFBD (Discrete Element Method-Multi Flexible Body Dynamics) bi-directional coupling technique. The EJM340 bolter miner was chosen as the research object, and a three-dimensional solid model of the bolter miner was built using the RecurDyn software. The cutting arm was flexibly modelled, and the tunnel model was built using the EDEM software. The motion parameters of the bolter miner and cutting head load were transferred through the bi-directional coupling interface to obtain the loads and stress parameters during the entire tunnel cutting process. Based on the stress-time variation, the fatigue life of the cutting arm was calculated, the overall damage and crack initiation locations were obtained, and the minimum number of cutting arm cycles was determined. The accuracy of the virtual model is verified through field experiments. The analysis results indicated that the crack emergence location and fatigue life obtained from the simulation were in agreement with the experimental results.

**Keywords:** Fatigue analysis / bolter miner / cutting arm / rigid flexible coupling simulation

## 1 Introduction

Bolter miners are used for low-stress coal tunneling by integrating tunneling, support, and transportation functions in one machine to achieve efficient tunneling [1]. They operate in harsh environments and are susceptible to fatigue failure because of their severe and continuous load cycles. Higher failure rates can increase downtime and adversely affect excavation efficiency and personnel safety. The cutting arm is a critical component of the bolter miner, and its fatigue life directly influences its performance.

Previous studies have conducted fatigue analyses of mining equipment. Zhen Tian et al. [2] established a rigid-flexible coupling model for a shearer. They predicted the fatigue life of the rocker arm shell, planetary carrier, and planetary shaft based on the rain flow counting method. Hao et al. [3] obtained the load spectrum by solving spatial mechanics equations and calculated the fatigue life of shearer body joint bolts in the Ansys workbench. Chen Hongyue et al. [4] used the Ncode software to calculate the fatigue life of a guiding support plate. They optimized the structure of the guiding support plate based on fatigue calculation results. Shi Jianguo et al. [5] performed a fatigue life calculation for the rocker arm of a coal mining machine based on the Palmagram-Miner linear cumulative damage law.

Previous studies have mainly adopted a single direction coupling approach to fatigue life prediction of critical components of mining equipment, while coal cutting and crushing are the results of multifactor coupling [6]. The geometric and kinematic parameters of the working mechanism, coal deposit conditions in the tunnel, and interaction between the cutting head and coal directly or indirectly affect the cutting and breaking process of the bolter miner. The DEM-MFBD (Discrete Element Method-Multi Flexible Body Dynamics) bi-directional coupling technology enables real-time information exchange between the tunnel, cutting head, and cutting arm and more accurately simulates the process of coal cutting by the bolter miner [7].

To overcome the limitations of existing fatigue analysis methods, a complete bolter miner simulation system, including a dynamic model and tunnel model, was established to simulate the operation process of the bolter miner. The fatigue damage and life of the cutting arm were

* e-mail: liangccteg@163.com

**Table 1.** Bolter miner parameters.

| Parameters | Value |
|---|---|
| Overall weight (t) | 103 |
| Dimension (L×W×H) (mm) | 11,640 × 5000 × 2600 |
| Cutting head diameter (mm) | 1150 |
| Cutting head width (mm) | 5200 |
| Total power (kW) | 742 |
| Ground pressure (MPa) | 0.27 |

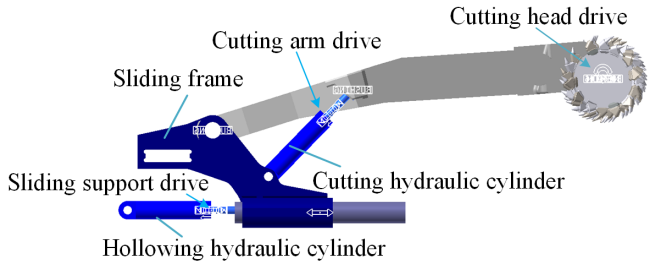


**Fig. 2.** Dynamics model.

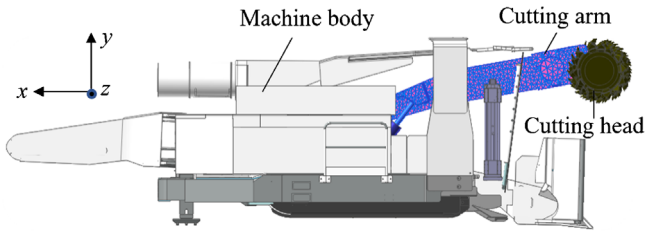


**Fig. 1.** Bolter miner model.

analyzed based on the rigid-flexible coupling technique [8] and the Palmgren-Miner criterion [9], and the accuracy of the virtual model was verified through experiments.

## 2 Simulation model

### 2.1 Bolter miner dynamic model

An EJM 340 bolter miner was used as the research object in this study. The technical parameters of bolter miners are listed in Table 1. A 3D model was created using SolidWorks based on the actual dimensions of the bolter miner. The model included a cutting head, cutting arm, and machine body. Unnecessary parts were removed to simplify the prototype. The model was then imported into the RecurDyn software, and the material properties, constraints, loads, and other simulation parameters were added for each part, as shown in Figure 1. The kinematic pair between the components is defined based on the definition of the kinematic pair in RecurDyn and the actual constraints during the operation of the bolter miner. Bushing forces were used to connect the cutting hydraulic cylinder to the cutting arm and the sliding support to the cutting arm instead of a revolutionary joint, to avoid redundant constraints. The stiffness of the rotation axis of the bushing force is set to 0. The constraints applied to the bolter miner dynamic model are shown in Figure 2 and Table 2.

The cutting arm was modelled as a flexible body to analyze the surface damage under alternating external loads. The finite element method was used to analyze the damage. Tetrahedral cells were used to mesh the member, and force-distributed rigid elements were used to connect rigid and flexible components. In total, 9468 nodes were created for the cutting arm. A modal reduction technique was employed to transform the finite element component into a modal flexible body. This method uses modal vectors

**Table 2.** Kinematic pair list.

| Connecting piece | Kinematic pair/force |
|---|---|
| Cutting arm, cutting head | Revjoint1 |
| Cutting hydraulic cylinder, sliding support | Revjoint2, Revjoint3 |
| Machine body, earth | Fixed1 |
| Cutting hydraulic cylinder, cutting arm | Bushing1, Bushing2 |
| Sliding support, cutting arm | Bushing3, Bushing4 |
| Cutting hydraulic cylinder piston, Cutting hydraulic cylinder barrel | TraJoint1, TraJoint2 |
| Hollowing hydraulic cylinder piston, Hollowing hydraulic cylinder barrel | TraJoint3 |
| Machine body, sliding support | TraJoint4 |
| Hollowing hydraulic, sliding support | Revjoint3 |
| Hollowing hydraulic, machine body | Revjoint4 |

and coordinates to describe elastic deformation, allowing modalities that contribute little to deformation to be neglected. This dramatically increases the computational speed while accurately describing the dynamic properties with fewer modal degrees of freedom. To ensure accuracy, this study considered the first 20 modes of the cutting arm. Figure 3 shows the first four vibration modes.

### 2.2 Tunnel model construction

#### 2.2.1 Material parameters and contact model

It is necessary to select relevant physical and mechanical parameters to accurately reflect the mechanical properties of an actual tunnel. The physical and mechanical parameters of the coal and the cutting heads are listed in Table 3. The contact model between the coal and cutting heads was the Hertz-Mindlin (no-slip) contact model, with the contact parameters listed in Table 4 [10].

#### 2.2.2 Mechanical parameters of coal particles

Because coal is in a massive structural state before cutting, and fragmentation occurs during the cutting process, some bonds must exist between the coal particles. The Hertz-Mindlin model with bonding was used to model the contact between coal particles in this study [11,12]. The model for

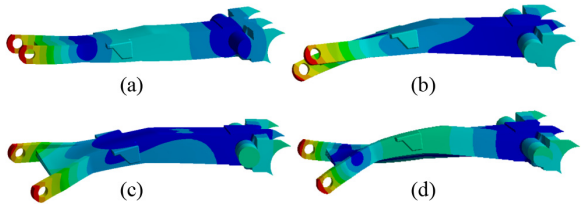


**Fig. 3.** Mode shapes of the cutting arm: (a) the first mode shape; (b) the second mode shape; (c) the third mode shape; (d) the fourth mode shape.

**Table 3.** Physical and mechanical parameters of coal and cutting head.

| Material | Density (kg/m$^3$) | Poisson's ratio | Shear modulus (MPa) |
|---|---|---|---|
| Cutting head | 7850 | 0.31 | 8100 |
| Coal | 1280 | 0.28 | 785 |

the bonding between two standard spherical particles, $a$ and $b$, with particle radii $R_a$ and $R_b$, respectively, is shown in Figure 4. The dotted area represents the cylindrical beam of the bonded structure. The cylindrical beam was a virtual area, with $O_c$ as the center of the cylinder. In this region, forces and moments can be transmitted between particles in contact with each other and can withstand certain tangential and normal motions. After bonding, the forces ($F_{n,t}$)/torques ($T_{n,t}$) on the particle were set to zero and adjusted incrementally at every time step according to equation (1) [13].

$$\begin{cases} \delta F_n = -v_n S_n A \delta_t \\ \delta F_t = -v_t S_t A \delta_t \\ \delta F_n = -\omega_n S_n \delta_t J \\ \delta T_t = -\omega_t S_n \delta_t J/2 \\ A = \pi R^2 \\ J = \dfrac{\pi}{2} R^4 \end{cases}, \tag{1}$$

where $\delta F_{n,t}$ are normal and tangential forces, respectively, $\delta T_{n,t}$ are normal and tangential moments, respectively, $\delta_t$ is the simulation step size, $S_{n,t}$ are the normal and tangential stiffnesses, respectively, $v_{n,t}$ are the normal and tangential velocities of the particle, respectively, $\omega_{n,t}$ are the normal and tangential rotational angular velocity of the particle, respectively, $A$ is the cross-sectional area of the bond region, $J$ is the polar moment of inertia of the bond, $R$ is the bond disk radius.

The bonding contact model can be used to bond particles with finite-sized "glue" bonds. This bond can resist tangential and normal movements up to a maximum normal and tangential shear stress, at which point the bond breaks. The maximum normal and tangential shear stresses can be described as follows [14]:

$$\begin{aligned} \sigma_{\max} &< -\frac{F_n}{A} + \frac{2T_t}{J} R \\ \tau_{\max} &< -\frac{F_t}{A} + \frac{T_n}{J} R \end{aligned}, \tag{2}$$

where $\sigma_{\max}$ and $\tau_{\max}$ are the critical normal stress and shear stress, respectively.

According to equations (1)–(2), the force-displacement characteristics of the bond are described by five main parameters:$S_{n,t}$, $\sigma_{\max}$, $\tau_{\max}$and $R$. These parameters can be obtained by fitting predictive equations to the rock mechanics parameters listed in Table 5 [1].

#### 2.2.3 Tunnel model

The tunnel was modelled with particles of 25 mm radius, with dimensions of $6 \times 1.2 \times 3.2$ m. When the bond formation time was reached, all defined particles in contact were bonded together, as shown in Figure 5.

## 3 DEM-MFBD bi-directional coupling simulation

### 3.1 Cutting operation flow

As shown in Figure 6, the cutting operation flow can be divided into four stages.

- The cutting head is activated, and the cutting arm rises to the top of the tunnel.
- The hollowing hydraulic cylinder drives the cutting arm forward to a feed depth of half the diameter of the cutting head, thereby achieving hollowing action.
- The cutting arm swings downwards.
- The hollowing hydraulic cylinder drives the cutting arm back to clear the bottom.

Stages (b) and (c) are the main stages of the cutting operation flow and account for most of the working time [15]. Therefore, only stages (b) and (c) were considered in the following simulations.

### 3.2 Simulation parameters

The drive applied to the bolter miner dynamic model is illustrated in Figure 2. The cutting head was rotated clockwise at constant angular speed to cut the tunnel. The cutting arm controls the position of the cutting head. The hollowing hydraulic cylinder drives the slide frame, cutting arm, and cutting head forward to achieve the hollowing action. The cutting hydraulic cylinder drove the cutting arm downwards to achieve cutting action. The driving functions are listed in Table 6.

### 3.3 Bi-directional coupling setting

The excavation process of a bolter miner is the result of multiple coupling factors. The working mechanism

**Table 4.** The parameters of contact properties of coal and cutting head.

| Materials parameters | Coefficient of restitution | Coefficient of static friction | Coefficient of rolling friction |
|---|---|---|---|
| Coal to coal | 0.5 | 0.6 | 0.05 |
| Coal to cutting head | 0.5 | 0.4 | 0.05 |

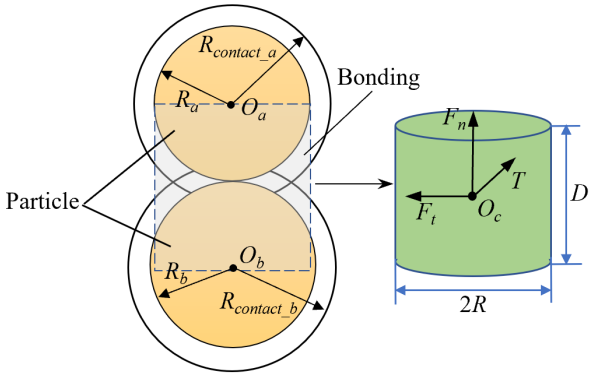


**Fig. 4.** Hertz-Mindlin model with bonding.

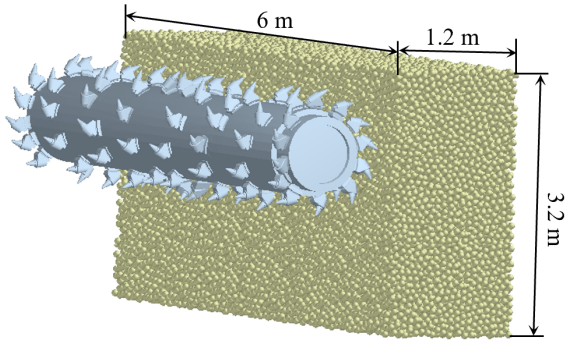


**Fig. 5.** Tunnel model.

**Table 5.** Particle adhesion parameters.

| Normal stiffness ($N/m^3$) | Tangential stiffness ($N/m^3$) | Critical normal stress (Pa) | Critical shear stress stress (Pa) | Bond disk radius (mm) |
|---|---|---|---|---|
| $4.5 \times 10^{10}$ | $1.8 \times 10^{10}$ | $3.2 \times 10^{6}$ | $3 \times 10^{6}$ | 28 |

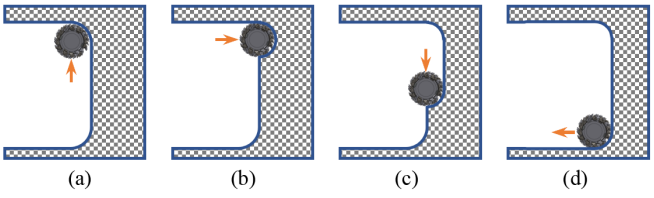


**Fig. 6.** Cutting operation flow (a) lifting cutting head; (b) feed hollowing; (c) downward cutting; (d) clearing bottom.

**Table 6.** Driving function settings.

| Drive | Type | Driving function |
|---|---|---|
| Cutting head drive | Velocity | Step(time,0,0,0.2,2.61) |
| Cutting arm drive | Displacement | Step(time,10,0,30,-360) |
| Sliding support drive | Displacement | Step(time,0,0,10,500) |

parameters, kinematic parameters, rock properties of the material, and interaction between the cutting head and the tunnel directly or indirectly influence the excavation process and dynamics of the bolter miner. Therefore, based on the principle of bi-directional coupling of DEM-MFBD, a bi-directional coupling model was established using EDEM and RecurDyn software.

The bi-directional coupling simulation of the EDEM-RecurDyn was performed at any time step of the EDEM. RecurDyn passes the kinematic parameters such as displacement, velocity, and acceleration of the coupling component obtained from the time step calculation to EDEM, which recalculates the effect of the coupling component position change on parameters such as the force, position, and velocity of the material particles. Based on discrete element theory, EDEM calculates the forces and moments of the material particles on the coupled components and transmits the data back to RecurDyn. RecurDyn recalculates the dynamic parameters of the coupled components based on the multibody dynamics theory and completes the bi-directional coupling transfer of the data. Information is exchanged between RecurDyn and EDEM in wall format files [16,17]. During operation, only the cutting head interacts with the tunnel; the remaining components do not interact with the tunnel. To improve the efficiency of the simulation, the cutting head 3D model was exported as a wall file using the export function in the External SPI module of RecurDyn, and the file was

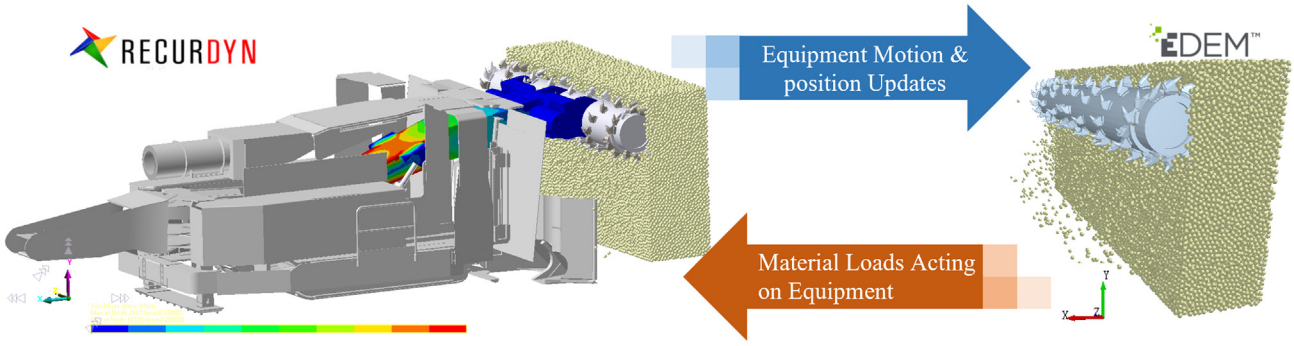


**Fig. 7.** EDEM-RecurDyn bi-directional coupling.

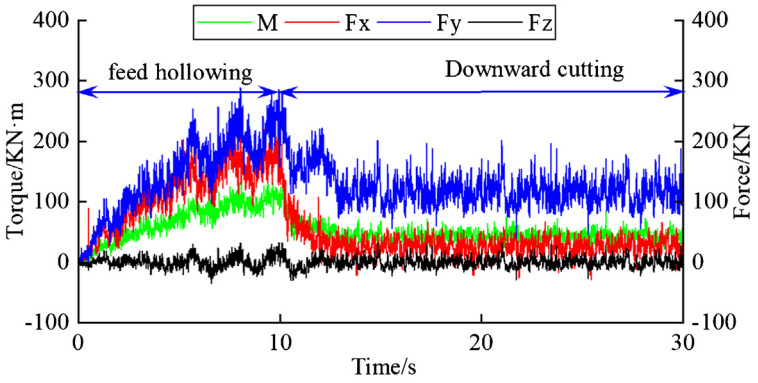


**Fig. 8.** Cutting load.

imported into the EDEM software. The bi-directional coupling simulation of the bolter miner is shown in Figure 7.

RecurDyn simulates the position and speed data of the cutting head in advance and then transfers it to EDEM, which is calculated at the same time point. This alternating mode continues until the simulation time reaches a specified end time [18]. Owing to the explicit time integration method implemented in the EDEM, multiple time steps are typically required to simulate the same periods as the individual time steps of RecurDyn. Therefore, the time steps may differ between the two solvers, but the simulation steps are the same [19]. Considering the actual computing power of the laboratory computer, the time steps of EDEM and RecurDyn were set to $1 \times 10^{-5}$ s and 0.01 s, respectively, with a total simulation time of 30 s.

## 4 Simulation result

### 4.1 Cutting load analysis

The loads acting on the cutting head are primarily composed of combined forces $F_x$, $F_y$ and $F_z$ in $x$-, $y$-, and $z$-directions, respectively, and moment $M$ along its axis. As shown in Figure 8, the external forces acting on the cutting head fluctuate owing to the random filling process of the coal seam particles. During the hollowing stage, the loads increased with increasing depth and reached their maximum values at a depth of 500 mm. During the cutting stages, the loads fluctuated steadily with amplitudes lower than those during the hollowing stages because the cutting depths were less than those during the hollowing stages.

### 4.2 Cutting arm stresses

Figure 9 shows the stress cloud of the cutting arm. The maximum stress point of the cutting arm is located where the cross-sectional shape of the cutting arm changes, specifically at node 2532. The maximum stress value is 162 MPa, less than the yield strength of the cut-off arm material ZG20SiMn (322.8 MPa), with a safety factor of 2. This part is classified as high circumferential fatigue.

Crack initiation and extension primarily occurred on the surface of the structure. Therefore, the structural stresses obtained from finite element analysis need to be transformed into stresses on the surface of the unit using the tensor transformation method. The stress-time variation at the surface nodes with the most severe damage to the cutting arm is shown in Figure 10. As the depth of the cut increased, the stress also increased. When $t$ =10 s, the hollowing depth is the largest, and the stress has the largest

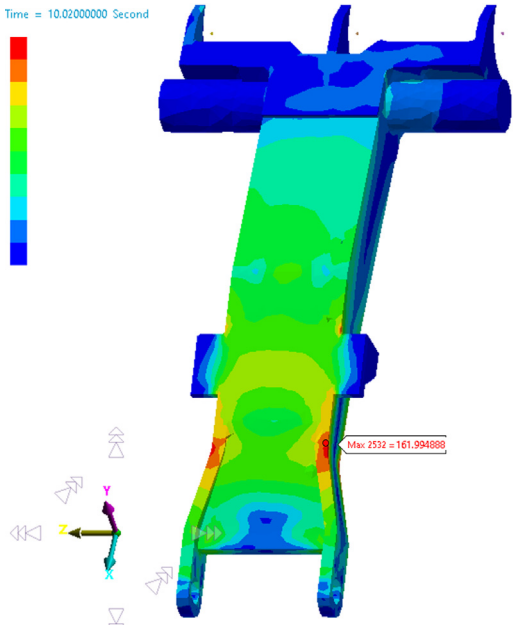


**Fig. 9.** Stress contour.

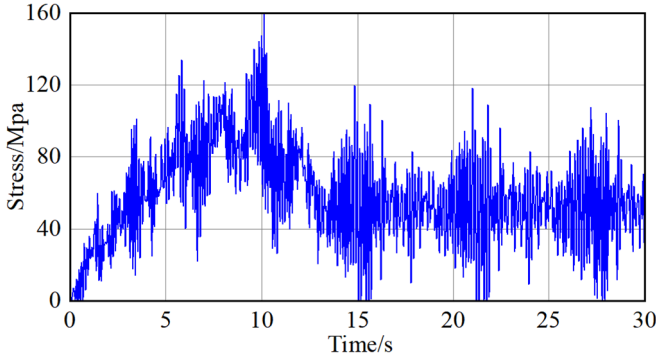


**Fig. 10.** Cutting arm stress-time history.

value at this time. At the initial stage of coal cutting, the stress tends to decrease and fluctuates within a specific range as the cutting continues. The load on the node is a randomly varying dynamic stress-time history, owing to the random excitation of the cutting head by the tunnel.

### 4.3 Rain flow counting

To calculate the life based on an S-N curve, external loads must be cyclic, and counting methods should be used to convert random loads into variable amplitude cyclic loads. The rain flow counting method is commonly used for fatigue analysis because it is practical and follows stress-strain hysteresis lines. This method assumes that random load spectra are based on the repeated load-time histories of typical load spectrum blocks. By identifying all load cycles contained in typical load spectrum blocks, random load spectra can be converted into variable amplitude load

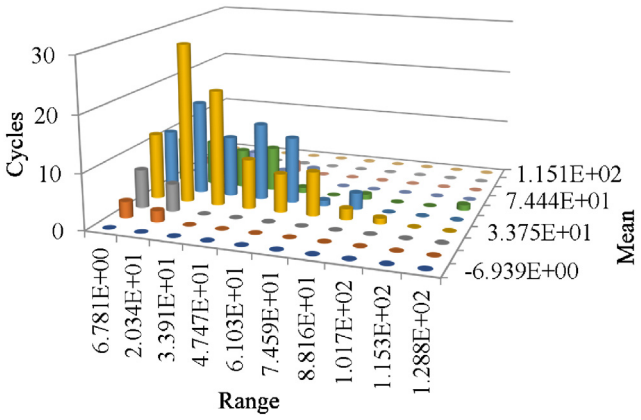


**Fig. 11.** Rain flowing counting results.

**Table 7.** Parameters of ZG20SiMn.

| Parameters | Value |
|---|---|
| Fatigue strength coefficient | 861 |
| Fatigue strength exponent | 0.09127 |
| Ultimate tensile strength (MPa) | 510 |
| Modulus of elasticity (MPa) | $2.08\times10^5$ |
| Poisson's ratio | 0.29 |

spectra consisting of a series of load cycles. Figure 11 shows a cyclic plot of the stress amplitude and average stress obtained by performing rain flow counting on the stress-time history in Figure 10.

### 4.4 S-N curve

The fatigue analysis of the cutting arm should be based on the S-N curve, which reflects the relationship between the applied stress and fatigue life of the cutting arm. Because the cutting arm has high circumferential fatigue, the S-N curve is plotted based on the Masson-Coffin life criterion, and the Masson-Coffin life equation is shown in equation (3) [20]

$$\frac{\Delta\sigma}{2} = \sigma'_f(2N_f)^b, \tag{3}$$

where $\frac{\Delta\sigma}{2}$ is normal stress amplitude for a cycle, $\sigma'_f$ is the fatigue strength coefficient, $2N_f$ is the reversals to failure, $b$ is the fatigue strength exponent.

A new database of the cutting arm material, ZG20SiMn, was created using RecurDyn, as presented in Table 7. The logarithms of both ends of equation (3) can be solved to obtain equation (4). The S-N fitting curve was generated according to a log-linear relationship. The S-N curve of equation (4) was corrected, and $W_F$ was calculated using equation (5). The values of the coefficients in equation (5) are listed in Table 8. The corrected S-N curves

**Table 8.** Parameter values of fatigue influencing factors.

| Parameters | $K_f$ | $m_s$ | $m_d$ | $m_t$ | $m_o$ |
|---|---|---|---|---|---|
| Value | 2 | 2 | 0.62 | 0.85 | 1 |

are shown in Figure 12.

$$lg\left(\frac{\Delta\sigma}{2}\right) = lg(861) - 0.09127lg(2N_f), \tag{4}$$

$$W_F = \frac{K_f}{m_s \times m_d \times m_t \times m_o}, \tag{5}$$

where $K_f$ is the stress concentration factor, $m_s$ is the surface factor, $m_d$ is the size factor, $m_t$ is the load factor, $m_o$ is the other factor.

Because the S-N curve can only reflect the fatigue life of the cutting arm under symmetric cyclic stress, it is difficult for the S-N curve to work well when the average stress value is not zero and the stress amplitude is not significant. Therefore, the Goodman method was used to modify the S-N curve by converting the non-zero average stress into an equivalent symmetric stress, as shown in equation (6) [21]

$$\frac{\sigma_a}{S_e} + \frac{\sigma_m}{S_u} = 1, \tag{6}$$

where $\sigma_a$ is the stress amplitude, $S_e$ is the effective alternating stress at failure for a lifetime, $S_u$ is the ultimate strength, $\sigma_m$ is the mean normal stress for a cycle.

### 4.5 Fatigue life calculation

Fatigue damage is caused by the accumulation of the fatigue damage caused by alternating loads. The components can be damaged under any stress, and the damage is permanent and cumulative. Fatigue failure occurs when cumulative damage causes a component to approach its fatigue-life limit. Linear damage accumulation theory assumes that the damage caused by each stress is independent and can accumulate linearly. Linear cumulative damage theory significantly simplifies the fatigue mechanism, making the calculation simple and accurate. Therefore, linear fatigue damage theory (Palmgren-Miner criterion) was used to calculate the total damage and fatigue life of the cutting arm. The Palmgren-Miner criterion defines the total damage of the material as $D$. The damage caused by a particular load cycle is $D_i = 1/N_i$. The total damage caused by $n$ load cycles was calculated using equation (7). After calculating the total damage value, the fatigue life was calculated using equation (8) [22]

$$D = \sum_{i=1}^{n} \frac{n_i}{N_i}, \tag{7}$$

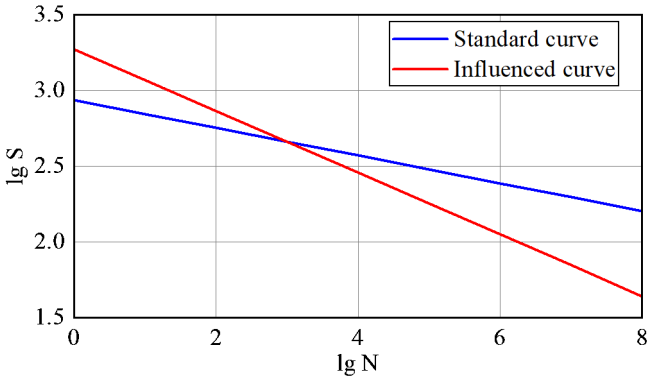


**Fig. 12.** S–N curve.

where $N_i$ is the fatigue life of the components under $\sigma_i$ and $n_i$ is the number of cycles under $\sigma_i$

$$\lambda = \frac{1}{D}, \tag{8}$$

where λ represents the fatigue life.

Figure 13 presents the life contour of the cutting arm using bolter miner hollowing-cutting as the minimum cycle of the operation flow. The part with the shortest life is shown in red and the part with the most extended life is shown in blue. The minimum number of nodes in the cutting arm cycle was 2532, and the cycle number was 652280. It was located where the cross-sectional shape of the cutting arm changed, and the fatigue damage value was $1.533e^{-6}$. Meanwhile, the life of the area where the ear mount and cutting arm are connected is relatively short. The fatigue-life contour pattern of the cutting arm is consistent with the stress contour. The fatigue life cloud diagram of the cutting arm is consistent with the stress cloud diagram. The tunneling depth is 0.5 m in one hollowing-cutting cycle of the bolter miner, and the total tunneling depth is 326140 m, calculated according to equation (9).

$$L = 0.5n, \tag{9}$$

where $L$ represents the depth of tunneling, $n$ is the number of cycles.

To verify the accuracy of the simulation results, experiments were conducted on a bolter miner in service at the tunneling face of the No. 2 coal mine of Huangling Mining Group Co., Ltd., China, as shown in Figure 14. When the tunneling depth reached 298432 m, fatigue cracks appeared on the surface of the cutting arm. The locations of the cracks are shown in Figure 13. The actual fatigue life was lower than the simulation result because the effects of the fracture and gangue in the tunnel were not considered in the simulation. However, the error was within a reasonable range. The actual crack location is consistent with the simulation results, which verifies the reasonableness and feasibility of the bi-directional coupling fatigue analysis method based on the DEM and MFBD.

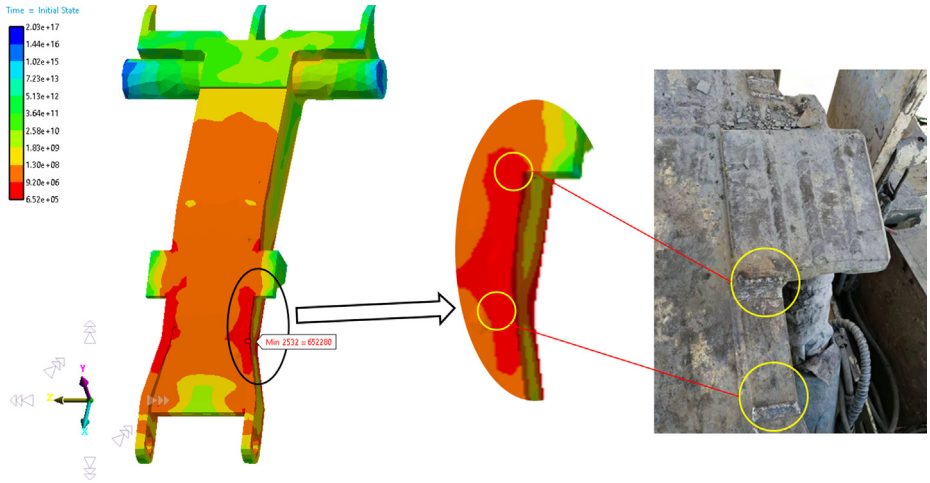


**Fig. 13.** Cutting arm life contour and actual fatigue damage location.

**Fig. 14.** Work site of bolter miner.

## 5 Conclusions

– A co-simulation based on Recurdyn-EDEM was used to obtain the stress-time history of the cutting arm during tunnel cutting. This approach effectively overcomes the shortcomings of static fatigue analysis methods with specific boundary conditions and loading history.
– In contrast to the traditional empirical method for predicting the fatigue life of a specific part, the Palmgren-Miner criterion was used to analyze the overall damage of the cutting arm. The shortest life was calculated as the change in the cross section of the cutting arm with a cycle count of 652280. The accuracy of the calculation method was verified by comparing it with experimental results.
– The effects of gangue and faults in the tunnel were not considered in the simulation, resulting in errors in the fatigue analysis results. Therefore, the next step in this study is to simulate a tunnel containing gangue and faults.

## Funding information

The financial supports from Chinese National Key R&D Program (Grant 2020YEB1314000).

## References

[1] X. Yang, D. Wu, X. Zou, H. Chen, S. Zhang, An analysis of digging anchor machine stability and track wear under digging conditions, Sci. Rep. **12**, 17738 (2022)
[2] Z. Tian, S. Gao, S.X. Jing, J. Li, Reliability and fatigue life analysis of key parts of shearer, Eng. Fail. Anal. **138**, 106357 (2022)
[3] Z. Hao, Y. Lei, J. Mao, Z. Yuan, Intensity analysis and fatigue life simulation for connecting bolt of shearer machine body, J. Syst. Simul. **29**, 1481 (2017)
[4] H. Chen, K. Zhang, M. Piao, X. Wang, J. Mao, Q. Song, Virtual simulation analysis of rigid-flexible coupling dynamics of shearer with clearance, Shock Vibr. **2018**, 1–18 (2018)
[5] J. Shi, G. Gao, R. Teng, Multi objective optimization of shearer drum parameters and its influence on strength of rocker arm, China Saf. Sci. J. **28**, 55 (2018)
[6] S. Qiao, Performance evaluation of different pick layouts on bolter miner cutting head, J. Mining Sci. **54**, 969–978 (2018)
[7] G. Zhao, J. Xiao, Q. Zhou, Fatigue models based on real load spectra and corrected SN curve for estimating the residual service life of the remanufactured excavator beam, Metals **11**, 365 (2021)
[8] X. Zhu, L. Pan, Z. Sun, Y. Wan, Y. Huang, J.-H. Choi, Simulation tool for dozer data acquisition, Autom. Constr. **142**, 104522 (2022)
[9] D. Pavlou, A deterministic algorithm for nonlinear, fatigue-based structural health monitoring, Computer-Aided Civil Infrastr. Eng. **37**, 809–831 (2022)
[10] J. Liu, C. Ma, Q. Zeng, K. Gao, Discrete element simulation of conical pick's coal cutting process under different cutting parameters, Shock Vibr. **2018**, 1–9 (2018)

[11] X. Liu, X. Li, X. Fu, X. Yang, J. Zhang, Analysis on the influence law of traction speed on the cutting performance of coal containing hard concretion, Mech. Ind. **24**, 5 (2023)
[12] X. Liu, C. Du, X. Fu, H. Zhao, J. Zhang, X. Yang, Wear analysis and performance optimization of drum blade in mining coal gangue with shearer, Eng. Failure Anal. **128**, 105542 (2021)
[13] X. Zhao, P. Zheng, L. He, M. Tao, Cutting edge preparation using the discrete element software EDEM, J. Br. Soc. Mech. Sci. Eng. **42**, 1–10 (2020)
[14] D.O. Potyondy, P. Cundall, A bonded-particle model for rock, Int. J. Rock Mech. Min. Sci. **41**, 1329–1364 (2004)
[15] Z. Xie, N. Zhang, D. Qian, C. Han, Y. An, Y. Wang, Rapid excavation and stability control of deep roadways for an underground coal mine with high production in Inner Mongolia, Sustainability **10**, 1160 (2018)
[16] G. Xu, H. Fang, Y. Song, W. Du, Optimal design and analysis of cavitating law for well-cellar cavitating mechanism based on MBD-DEM bidirectional coupling model, Agriculture **13**, 142 (2023)
[17] L. Shi, W. Zhao, C. Hua, G. Rao, J. Guo, Z. Wang, Study on the intercropping mechanism and seeding improvement of the cavity planter with vertical insertion using DEM-MBD coupling method, Agriculture **12**, 1567 (2022)
[18] Y. Li, Z. Hu, F. Gu, B. Wang, J. Fan, H. Yang, F. Wu, DEM-MBD coupling simulation and analysis of the working process of soil and tuber separation of a potato combine harvester, Agronomy **12**, 1734 (2022)
[19] Z. Liu, G. Wang, W. Guan, J. Guo, G. Sun, Z. Chen, Research on performance of a laboratory-scale SAG mill based on DEM-EMBD, Powder Technol. **406**, 117581 (2022)
[20] S. Marco, W. Starkey, A concept of fatigue damage, Trans. Am. Soc. Mech. Eng. **76**, 627–632 (1954)
[21] R. Gujar, S. Bhaskar, Shaft design under fatigue loading by using modified goodman method, Int. J. Eng. Res. Appl. **3**, 1061–1066 (2013)
[22] J.J. Kauzlarich, The Palmgren-Miner rule derived, Tribol. Ser. **14**, 175–179 (1989)

**Cite this article as**: A. Li, B. Wang, T. Wang, Z. Guo, Z. Yan, Effects of cutting head load on fatigue life of bolter miner cutting arm, Mechanics & Industry **24**, 22 (2023)